ENVIRONMENTAL RESEARCH
LETTERS

LETTER • OPEN ACCESS

Arctic sea ice modulation of summertime heatwaves over western North America in recent decades

ENVIRONMENTAL RESEARCH
LETTERS

CrossMark

OPEN ACCESS

RECEIVED
5 February 2022

REVISED
29 May 2022

ACCEPTED FOR PUBLICATION
7 June 2022

PUBLISHED
23 June 2022

LETTER

Arctic sea ice modulation of summertime heatwaves over western North America in recent decades

Houwen Wang[1], Yang Gao[2,*], Yuhang Wang[3,*] and Lifang Sheng[1]

[1] College of Oceanic and Atmospheric Sciences, Ocean University of China, Qingdao 266100, People's Republic of China
[2] Frontiers Science Center for Deep Ocean Multispheres and Earth System, and Key Laboratory of Marine Environment and Ecology, Ministry of Education, Ocean University of China, and Qingdao National Laboratory for Marine Science and Technology, Qingdao 266100, People's Republic of China
[3] School of Earth and Atmospheric Sciences, Georgia Institute of Technology, Atlanta, GA 30332, United States of America
[*] Authors to whom any correspondence should be addressed.

E-mail: yanggao@ouc.edu.cn **and** yuhang.wang@eas.gatech.edu

Keywords: heatwaves, sea ice, teleconnection, quasi-barotropic ridges

Supplementary material for this article is available online

Abstract

A catastrophic heatwave struck North America (NA) in the summer of 2021, the underlying cause of which currently remains unclear. The reanalysis data (1980–2021) is analyzed to elucidate the mechanism modulating the summer heatwaves. We find the heatwaves over western NA tend to occur concurrently with quasi-barotropic ridges (QBTRs). The 2021 record-breaking heatwave, in particular, coincides with an extended eight-day QBTR event. The frequency of QBTRs is modulated by large-scale forcing. During the period of 1980–2000, it is correlated with the Arctic Oscillation. After 2000, however, the QBTR frequency is highly associated with sea ice variations. Specifically, the negative sea ice anomalies in the Chukchi Sea are usually associated with stronger net surface shortwave radiation and low cloud cover, triggering upward motion and a low-pressure center in the low- and mid-troposphere. The low pressure strengthens a stationary wave response, concomitant with two alternately high- and low-pressure centers, inducing more frequent QBTRs over western NA. These findings indicate that further Arctic sea ice loss under a warming climate will likely lead to more devastating heatwaves over western NA.

1. Introduction

Heatwaves are extreme weather events with high temperatures, causing considerable damages to ecosystems and humans (Smoyer-Tomic *et al* 2003, Bondur, 2011, Pearce and Feng 2013, von Biela *et al* 2019). A severe heatwave event can result in thousands of deaths (Stefanon *et al* 2012). Heatwaves also have substantial effects on morbidity, including acute renal failure, diabetes, and cardiovascular diseases (Knowlton *et al* 2009). In the summer of 2021, a record-breaking heatwave swept across western North America (NA) from late June to early July. More than 500 people died during the event, and 180 wildfires occurred in British Columbia, Canada, amid a record-breaking temperature as high as 49.6 °C on 29 June 2021 (Schiermeier 2021). Therefore, it is of great significance to investigate the causes of heatwaves.

It has been suggested that heatwaves can be attributed to persistent anticyclones (Fischer *et al* 2007, Stefanon *et al* 2012). At the middle and high latitudes, the quasi-stationary atmospheric blocking is the primary weather system of anomalous anticyclone (Barriopedro *et al* 2011, Gao *et al* 2015, Schaller *et al* 2018, Li *et al* 2020). The duration and frequency of atmospheric blocking can be steered by the intensity of baroclinicity and upper-level zonal wind (Yao *et al* 2017). At lower latitudes, the intensity and duration of heatwaves are strongly modulated by subtropical highs such as the West Pacific subtropical high (Li *et al* 2015) and subtropical ridges in Europe (Sánchez-Benítez *et al* 2018). However, few studies investigated the distinct effects of anticyclones with different baroclinicity or dynamical properties on heatwaves.

The frequency and duration of heatwaves have been increasing and are projected to continue to increase even more substantially in a warming climate (Gao *et al* 2012, Habeeb *et al* 2015, Zhang *et al* 2018). Notably, Arctic warming has been about twice the global average in the past few decades (Screen and Simmonds 2010). For instance, the Arctic sea ice extent has declined at a rate of 4% per year from 1979 to 2010 (Cavalieri and Parkinson 2012), and its thickness in 2008 has almost halved compared with 1980 (Kwok and Rothrock 2009). The sea ice decline can induce more persistent and extreme mid- and high-latitude weather and atmospheric circulations (Vihma 2014, Yeo *et al* 2014, Coumou *et al* 2015, 2018, Overland *et al* 2016, Cvijanovic *et al* 2017, Kim *et al* 2020, Zou *et al* 2021). For example, the local effect behaves as the enhanced energy transfer from the ocean to the atmosphere, which may strengthen the warming and moisture locally, increasing the thickness of the lower troposphere (Screen *et al* 2013), whereas the sea ice loss may remotely lead to a decrease in the meridional temperature gradient and upper-level zonal wind speed at mid-latitude while stimulating Rossby wave trains (Francis and Vavrus 2012, Wang and He 2015, Zou *et al* 2020). The suggested relationship between sea ice decline and persistent mid and high-latitude weather patterns, and the strong dependence of heatwaves on persistent anticyclones inspires us to investigate the linkage between sea ice loss and heatwaves. Budikova *et al* (2019) find that the decrease in summer sea ice in Hudson Bay is associated with the increase in the frequency of summer heatwaves in the United States. Nevertheless, the mechanism of Arctic sea ice variations modulating heatwaves over western NA remains unclear.

In this study, we analyze the long-term reanalysis data (1980–2021) to diagnose the occurrences of large-scale high-pressure ridges and investigate their relationships with heatwaves over western NA and large-scale forcing factors such as the Arctic sea ice variations in recent decades. An emphasis is placed on decadal changes and the underlying processes.

2. Data and methods

ERA5 global hourly reanalysis (Hersbach *et al* 2020), with a horizontal resolution of 0.5° × 0.5°, is downloaded from Copernicus Climate Data Store (https://cds.climate.copernicus.eu/#!/home; last access: 14 November 2021) in ECMWF. This dataset is mainly used for (a) heatwave detection from near-surface 2 m air temperature, (b) ridge detection from geopotential height at 500 hPa (Z500), (c) correlation and composite analysis from 2 m temperature and Z500, (d) calculation of atmospheric baroclinicity from zonal wind speed at different altitudes, i.e. 200–400 hPa and 600–850 hPa, and (e) investigation of air-sea interaction from medium cloud cover, surface net longwave radiation and air temperature in the troposphere (1000–500 hPa). Monthly AO index is downloaded from Climate Prediction Center (CPC, www.cpc.ncep.noaa.gov/data/; last access: 14 November 2021).

According to the previous method (Li *et al* 2020), regional heatwaves are identified as continuous three or more days with daily maximum 2 m surface air temperature (Tmax) averaged over a region exceeding a certain threshold. The threshold is calculated for each calendar day of a year, equivalent to the 90th percentile of the Tmax on a 31 days moving window centered on that day during 1980–2009, warranting a sufficient sample size. The region is selected in western NA (green quadrilateral in figure 1(a)).

To identify the daily high-pressure ridges over NA, we develop an algorithm based on the method to detect troughs (Li *et al* 2018). Specifically, we first obtain the daily geostrophic curvature for each grid calculated by Z500 over NA. A ridge over a region can then be identified when the geostrophic curvature of each grid is negative and exceeds a certain threshold, and the width of the adjacent grids in the north-south direction is longer than a designated length threshold. The ridge detection method is summarized as follows:

(a) A spatial smoothing to Z500, at a spatial extent covering 20° in both zonal and meridional directions, is applied to reduce the impact of meso- and small-scale weather systems.
(b) The zonal and meridional components of geostrophic wind are calculated in equation (1) shown below, which can then be used to calculate the angle of the geostrophic wind. In a natural coordinate system, the curvature is, by convention, negative (positive) when a flow is anticyclonic (cyclonic), according to Holton (2004). Thus, the curvature of each grid point is calculated as the additive inverse of the rate of change in the geostrophic angle along the direction of the geostrophic wind, followed by a spatially moving average spanning 5° × 5° in latitudinal and longitudinal directions to eliminate minor disturbances. More details can be found in Li *et al* (2018)

$$u_g = -\frac{1}{f}\frac{\partial \Phi}{\partial y} \quad v_g = \frac{1}{f}\frac{\partial \Phi}{\partial x} \tag{1}$$

where u_g and v_g represent the latitudinal and meridional components of geostrophic wind speed, respectively, Φ denotes Z500, x and y denote latitudinal and meridional directions, and f denotes Coriolis parameter.
(c) In weather charts, a ridge is an extended region of relatively high atmospheric pressure, generally detected by the distribution of isobars convex towards areas of low values along local minimal curvature. Based on the shape of isobars and the distribution of the curvature calculated above, the threshold of geographic curvature is set to −0.05 (supplementary figure S1).

(d) Considering that the wavelength of synoptic-scale ridges is in the order of 1000–6000 km (Lackmann 2011) and the minimum spatial scale of atmospheric blocking approximates to 15° (Pelly and Hoskins 2003), a north-south width at 1500 km is set to be the length threshold. To avoid false ridges due to east-west subtropical highs, the north-south width of the ridges should be greater than the east-west width if the ridges are located south of 45° N, considering the position of subtropical highs documented previously (Wallace and Hobbs 2006, Hartmann 2015) as well as shown in supplementary figure S2.

High-pressure ridges are classified based on background baroclinicity, according to Yao *et al* (2017). The background baroclinicity is considered the vertical wind shear in the troposphere, calculated as the difference between the upper (200–400 hPa) and lower (600–850 hPa) zonal mean wind speed over NA (30°–70° N, 60°–150° W). A quasi-baroclinic ridge (QBCR) and a quasi-barotropic ridge (QBTR) are identified when a high-pressure ridge is detected, and the background baroclinicity on that day is the upper 75th percentile and lower 25th percentile during summer 1980–2021, respectively.

Moreover, longer-lasting QBTR events may yield a much more significant impact than a single-day event. Considering QBTRs and atmospheric blocking have similar effects on heatwaves in summer, following the work of Pelly and Hoskins (2003) and Small *et al* (2014), a QBTR event is defined when at least five continuous days are considered QBTR days, and a relaxation criterion is adopted when one day gap occurs in between two QBTR days, which is considered a QBTR day as well. A detailed check indicates minimal chances when a five day QBTR event is due to the filling of two day gaps. To facilitate the discussion, the middle day of each event is considered as the peak, defined as day 0, with the days before or after denoted by negative or positive numbers.

3. Results

3.1. Atmospheric circulation associated with regional heatwaves over NA in 2021

A long-lived and record-breaking regional heatwave event is detected in western NA from 22 June to 5 July 2021. To understand the spatial and temporal characteristics of the heatwave event, the Tmax anomaly, over each grid, relative to the climatological (1980–2009) mean on the respective day is calculated, with the temporal mean shown in figure 1(a) (shading), exhibiting strong positive anomalies over western NA. The strong high temperature in this area is concurrent with a large-scale ridge based on the mean geopotential height at 500 hPa centered on the northwestern United States (blue contour lines in figure 1(a)). Particularly, Tmax anomalies reach 13.0 °C, yielding the Tmax value of 36.8 °C on June 29 over southwestern Canada (i.e. grey box in figure 1(a)), located in the ridge center. Besides the heatwave period, most of the remaining days during summer 2021 show a positive anomaly relative to the climatological mean (figure 1(c)), indicative of high mean temperature even from a seasonal scale when regional heatwaves occur.

To this end, we delve into the association between regional heatwaves and summer mean air temperature. The ranking in percentile of summer mean Tmax in 2021 relative to 1980–2021 is displayed in figure 1(b). A striking feature is that most grids exceeding the 90th percentile are similar to the region where the record-breaking heatwave occurs over western NA (green quadrilateral in figure 1(b), the same as green quadrilateral in figure 1(a)). The interannual variations of summer mean Tmax averaged over western NA during 1980–2021 (black line in figure 1(d)) is further displayed together with the frequency (orange bars in figure 1(d)) and mean duration (red dots in figure 1(d)) of regional heatwaves over western NA, showing statistically significant correlations with coefficients of 0.77 ($P < 0.01$) and 0.53 ($P < 0.01$).

3.2. Relationship between ridges and summer mean Tmax in summer

To quantitatively analyze the linkage between the ridges and the summer mean Tmax over western NA (green quadrilateral in figure 1(b)), high-pressure ridges during summer 1980–2021 are first identified over NA. The different types of ridges are classified based on atmospheric baroclinicity, such as QBTRs and QBCRs (see section 2 for definitions). Detrending is applied before the time-series analysis in this study to avoid the influence of linear trends. The total number of summer QBTR days over each grid of NA is regressed onto the standardized summer mean Tmax averaged over western NA during 1980–2021, showing strong linkage in the west of NA (referred to as WNA; dark blue square in figure 2(a)).

Further examination of the number of summer QBTR days over WNA and summer mean Tmax over western NA (green quadrilateral in figure 1(a)) depicts a statistically significant correlation of 0.49 ($P < 0.01$). In addition, the abovementioned analysis in this section has been repeated using QBCRs, implying no significant relationship with summer Tmax. The greater role of QBTRs in summer mean Tmax may be explained by decreased baroclinity associated with weaker upper-level flows, retarding the movement of ridges and prolonging the life cycle of the weather systems (Inoue *et al* 2012).

To further examine the impact of atmospheric baroclinicity on heatwaves, in addition to the number of QBTR days, the longer-lasting ridges such as QBTR events may facilitate a more persistent and widespread invasion of high temperatures. We define a

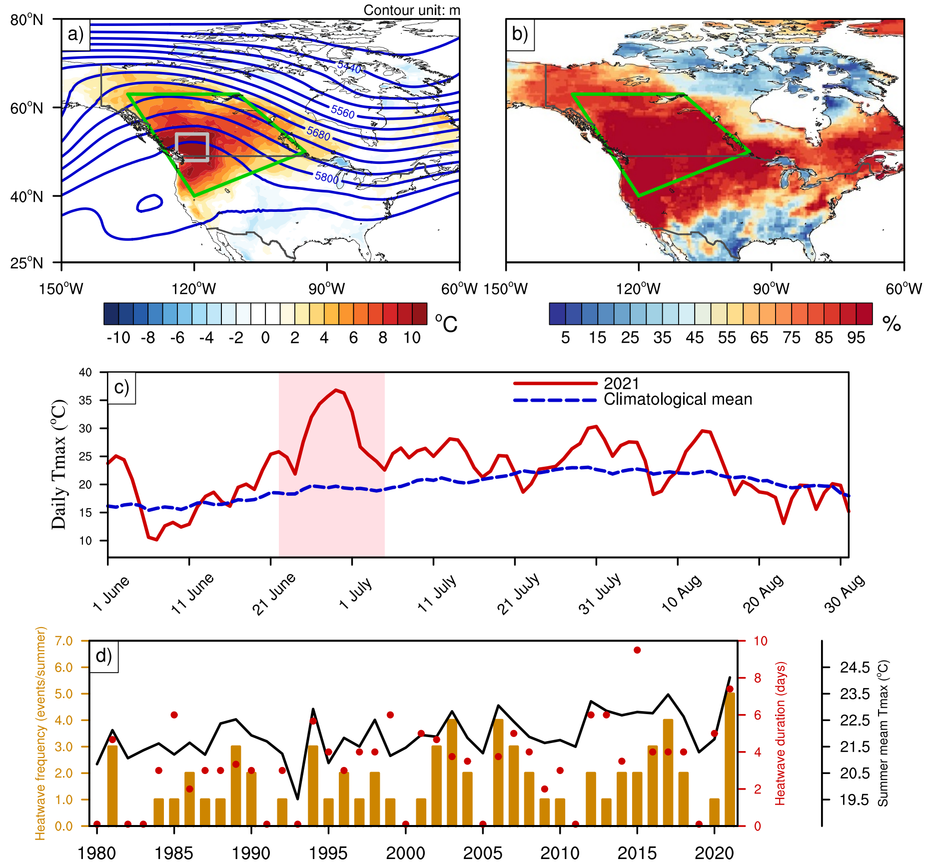

Figure 1. Temporal and spatial characteristics of the record-breaking regional heatwaves and summer mean Tmax. (a) Composited daily Z500 (contour, interval = 40; unit: m) and Tmax anomalies (shading; unit: °C) from 22 June to 5 July 2021. Regional heatwaves are detected in the region inside the green quadrilateral. (b) Percentile of summer mean Tmax in 2021 across about 40 year summers during 1980–2021. The green quadrilateral in figure (b) is the same as that in figure (a). (c) Daily Tmax in 2021 (solid red line) and daily climatological mean Tmax during 1980–2009 (dashed blue line) averaged over southwestern Canada (grey box shown in figure (a)), and shading in pink is indicative of the period when regional heatwaves occur. (d) Summer mean Tmax (black line) and regional heatwave frequency (orange bars) and duration (red dots) over western NA (green quadrilateral in figure (a)) during summers from 1980 to 2021.

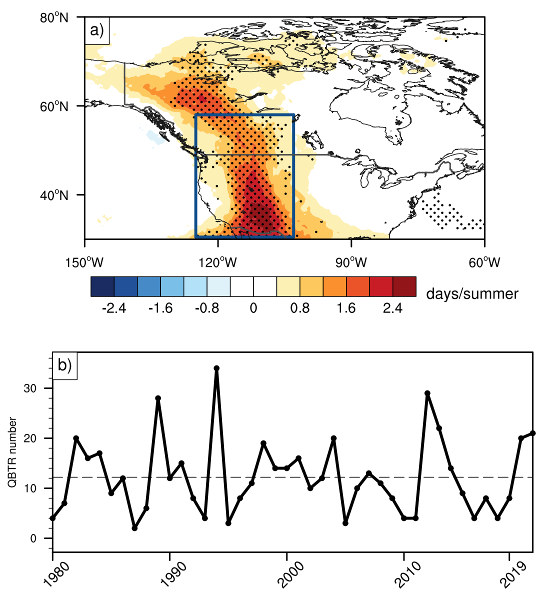

Figure 2. The relationship between summer mean Tmax and the number of summer QBTR days. (a) The number of summer QBTR days at each grid (unit: days/summer) regressed onto the standardized summer mean Tmax averaged in green quadrilateral in figure 1(b) during 1980–2021 after detrending. (b) Variations of the number of summer QBTR days over WNA during 1980–2021, showing no significant trend. The horizontal dashed reference line denotes the climatological mean of QBTRs during summer 1980–2009.

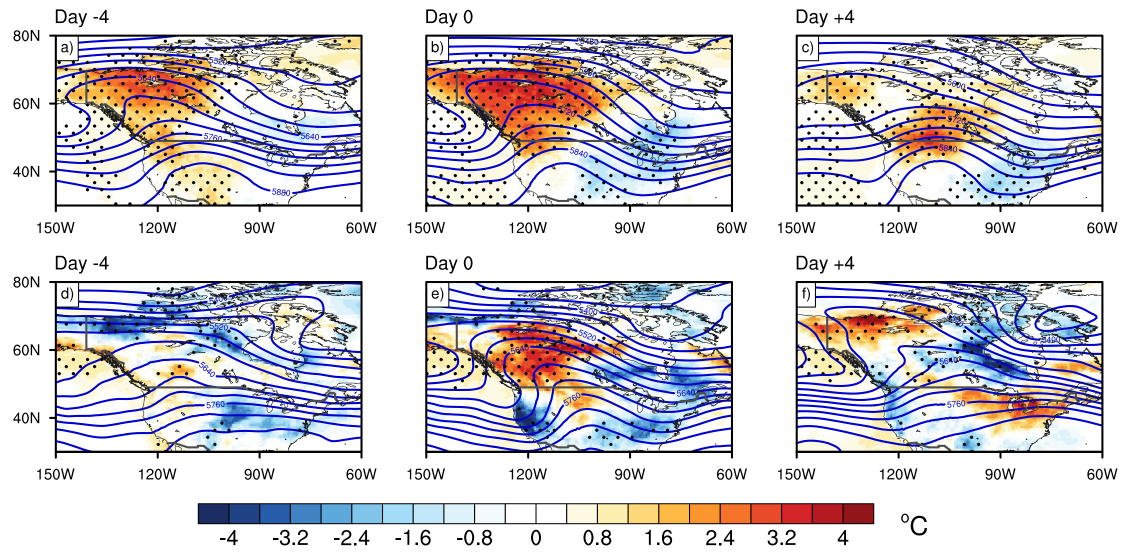

Figure 3. Composited daily Tmax anomalies compared to 1980–2009 (shading, unit: °C) and Z500 (contour, interval = 40; unit: m) on day −4, day 0 and day +4 for QBTR events (a)–(c) and QBCR events (d)–(f). Black stippling denotes areas with statistical significance at 0.05.

QBTR event over WNA (dark blue box in figure 2(a)) at least five days (see section 2) and detect a total of 36 events on average lasting 8.4 days per event (referred to as duration) during summer 1980–2021. Notably, a long-lasting QBTR event is detected over WNA from 25 June to 2 July 2021, well-matched in time with the record-breaking heatwave over western NA (22 June to 5 July 2021). Based on the mean QBTR event duration, we composite Z500 and Tmax anomalies relative to climatological mean from 1980 to 2009 during day −4 to day +4 (day 0 is the peak of QBTR events, defined in section 2) to analyze the impact of QBTR events on the spatial and temporal variations of Tmax (figures 3(a)–(c)). Widespread positive Tmax anomalies across western NA are induced by QBTRs, particularly in the belts across northwestern Canada to northwestern United States. During day −4 to day +4 of the 36 QBTR events, 47% (17 times) is concomitant with regional heatwaves occurring in western NA. The probability of the co-occurrence of QBTR events and regional heatwaves shows a nicely monotonical increase by perturbing the threshold used to define QBTR events, e.g. from 47% (abovementioned five days threshold) to 44% (three days), 57% (six days), 65% (eight days) and 67% (ten days).

Similarly, QBCR events (e.g. a threshold of five days) are detected and composited during day −4 to day +4 (figures 3(d)–(f)), with a total number of 12 events from 1980 to 2021. The QBCR events only cause a increase in Tmax beneath the location of QBCRs, the amplitude of which is weaker than the QBTR (figures 3(a)–(c) vs. (d)–(f)). The occurrence probability of regional heatwaves over western NA is only 25% during QBCR events. Hence, the persistent ridges concurrent with weaker baroclinicity (e.g. QBTRs) are more conducive to heatwaves over western NA.

3.3. The mechanism modulating the QBTRs and heatwaves

Next, we investigate the dynamic origins in the Arctic modulating the interannual variations in summer QBTRs over WNA (figure 2(a)). As the leading mode of large-scale atmospheric circulation in the northern hemisphere (Thompson and Wallace 2000), AO is firstly correlated with the number of QBTR days in summer during 1980–2021, showing a statistically significant correlation of 0.34 ($P < 0.05$). Moreover, considering the intermittent effects of large-scale forcing or circulation on mid-latitude weather (Overland *et al* 2016), a 21 year moving correlation is further applied between AO and the number of QBTR days. Although the correlation coefficient of 0.34 during 1980–2021 is relatively low, the moving correlation (i.e. 0.64 during 1980–2000) exhibits a more significant correlation prior to 2001 but decreases sharply thereafter (red line in figure 4(a)), indicative of weakened effects of AO on QBTRs in the latter half period.

As was documented earlier, a QBTR over western America is induced in 2007 due to the substantially lower sea ice compared to the other years from 1979 to 2008 (Strey *et al* 2010). Similarly, the location of ridge peaks is also suggested to be driven by sea ice loss (Francis and Vavrus 2012). To understand the Arctic modulating the QBTRs in the latter 21 years from 2001 to 2021, the regression between the Arctic sea ice and interannual variations in the number of summer QBTR days is evaluated each month during 2001–2021. The regression pattern of June sea

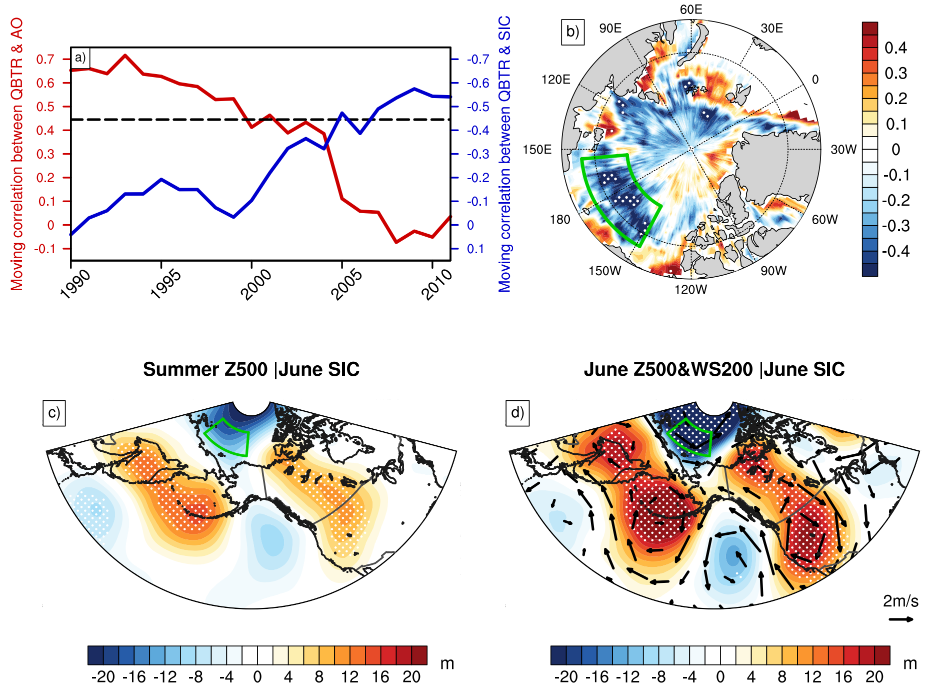

Figure 4. (a) Twenty-one year moving correlation between the number of summer QBTR days passing over WNA (dark blue square in figure 2(a)), and summer AO index (solid red line) and sea ice concentrations (SIC, solid blue line) in June averaged in the Chukchi Sea (green circular sector in figures (b)–(d)) during 1980–2021. The numbers in the abscissa represent the center of the 21 year used in the calculation of moving average. The dashed horizontal line demarcates the significance of the correlation coefficient, with values on top of the line implicative of significance ($P < 0.05$). (b) Correlation pattern between the number of summer QBTR days over WNA and SIC in the Chukchi Sea in June during 2001–2021. Regression of (c) geopotential height (unit: m) at 500 hPa in summer, (d) geopotential height at 500 hPa (unit: m) and wind speed at 200 hPa (unit: m s^{-1}) in June against the additive inverse of standardized SIC averaged in the Chukchi Sea during June 2001–2021. White stippling denotes areas with statistical significance at 0.05. Linear trends are removed from the analysis.

ice displays a significant negative correlation (-0.56; $P < 0.01$) in the Chukchi Sea (green circular sector in figure 4(b)). A 21 year moving correlation between the sea ice concentrations in June over this circular area and the number of summer QBTR days is further conducted (blue line in figure 4(a)). The continuous enhancement in the moving correlation with the largest one of -0.58 centered in 2009 confirms the more significant effect of sea ice variations modulating the number of summer QBTR days during 2001–2021. The very low moving correlation (0.04) in 1990 indicates the negligible impact of sea ice concentrations on QBTRs at the end of the last century, such as 1980–2000.

To investigate how sea ice variations may intensify regional heatwaves in western NA, the summer geopotential height anomalies at 500 hPa are regressed onto the additive inverse of standardized sea ice concentrations averaged in the Chukchi Sea during June 2001–2021 (figure 4(c)). A stationary wave response, with two striking high-pressure centers over the Bering Sea and western NA and two relatively weak low-pressure centers over the Gulf of Alaska and southeast side of the Sea of Okhotsk, occurs along the North Pacific at mid-high latitudes, concomitant with a low-pressure center over the Chukchi Sea. This stationary wave is barotropic, presenting similarly low- and high-pressure centers from 925 hPa to 200 hPa. The high pressure over WNA, to some extent, implies potential connections between negative sea ice anomalies and enhanced QBTRs over WNA. Furthermore, the regression pattern of geopotential height at 500 hPa and wind speed at 200 hPa in June (figure 4(d)) shows that the low-pressure center over the Chukchi Sea, triggered by reduced sea ice, induces westerly anomalies on its southern flank, strengthening the high-pressure center over the Bering Sea in the stationary waves. This response is stronger than the other three anomalous centers in the stationary wave, facilitating the wave activity along the jet stream and resulting in more frequent QBTRs in WNA. In addition, the horizontal structure of stationary wave resembles the part of the Pacific-Japan pattern located over the North Pacific at mid-high latitudes (Nitta 1987). Teng *et al* (2013) also suggest a similar wave train over the North Pacific facilitating the formation of heatwaves over US.

The regression pattern abovementioned supports the linkage between Arctic sea ice in the Chukchi Sea and increased QBTRs over WNA. The potential physical mechanism of the sea ice variations triggering the low-pressure center is further examined. As was demonstrated by Chang (2009), diabatic heating plays a major role in the maintenance of stationary waves. Previous studies have demonstrated

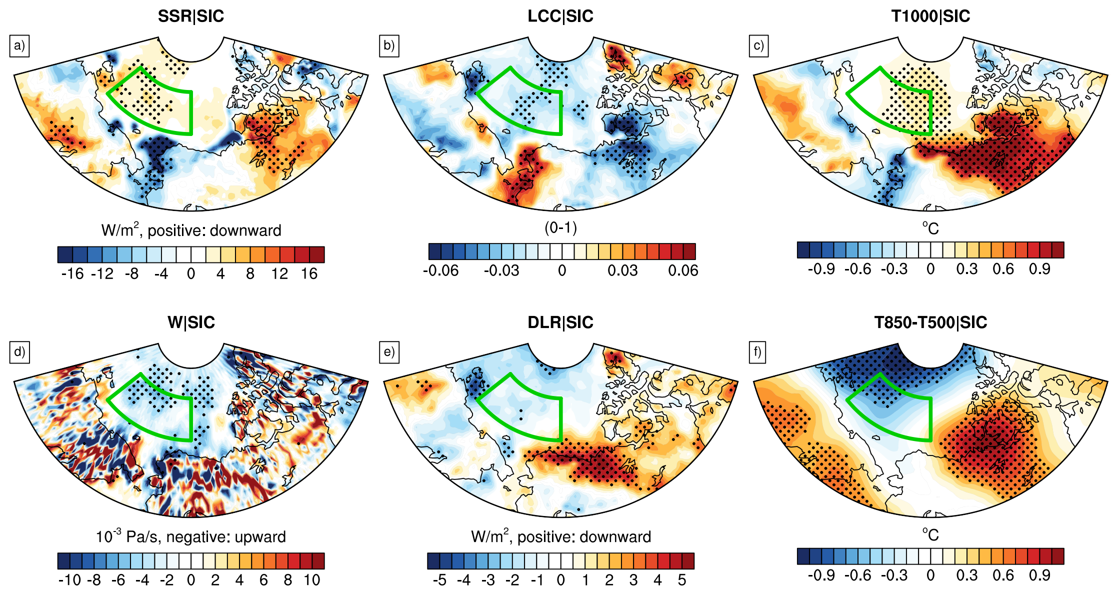

Figure 5. The mechanism of negative sea ice anomalies in the Chukchi Sea triggering a low-pressure center. Regression of (a) net surface shortwave radiation (SSR, unit: W m^{-2}), (b) low cloud cover (LCC, unit: 0–1), (c) air temperature at 1000 hPa (T1000, unit: °C), (d) vertical velocity (W, Pa s^{-1}), (e) downward long-wave radiation (DLR, unit: W m^{-2}) and (f) vertical average of air temperature from 850 hPa to 500 hPa (T850-T500, unit: °C) against the additive inverse of standardized sea ice concentrations averaged in the Chukchi Sea during June 2001–2021. Green circular sectors represent the Chukchi Sea. Black stippling indicates areas with statistical significance at 0.10. Linear trends are removed from the analysis.

that Arctic sea ice anomalies can affect the weather systems at mid latitude in summer by stimulating Rossby wave trains (Yin *et al* 2019b, 2020, Du *et al* 2022). For instance, Yin *et al* (2019a) found that the sea ice reduction in the Chukchi Sea combined with positive SST anomalies could trigger a stationary wave response at mid latitude, steering the atmospheric circulation over the west coast of NA. Therefore, the possible meteorological variables related to diabatic heating (figures 5(a)–(f)) are regressed onto the additive inverse of standardized sea ice concentration averaged over the Chukchi Sea in June 2001–2021. Stronger surface net shortwave radiation and decreased low cloud cover are conducive to negative sea ice anomalies (figures 5(a) and (b)), concurrent with increased air temperature at 1000 hPa (figure 5(c)). The increased air temperature causes an upward motion in the low and middle troposphere (figure 5(d)), favoring the formation of the low-pressure center (He *et al* 2018). Furthermore, decreased low clouds reduce the absorption of upward long-wave radiation in the mid-troposphere and emission of downward long-wave radiation (figure 5(e)), decreasing the temperature therein (Slingo and Slingo 1988), as well as shown in figure 5(f), further facilitating the formation of the low-pressure center (figure 4(d)). This structure with relatively cold air at high altitudes and warm air at low altitudes reduces the atmospheric stability (Wallace and Hobbs 2006), continuously maintaining the low-pressure center. Comparably, based on numerical experiments, He *et al* (2018) found a similar mechanism between the Artic sea ice anomalies over the Barents Sea in June and stationary wave response in summer over Eurasia, further warranting the robustness of the finding in this study. While the dynamic process is plausible, detailed modeling analysis is necessary in future to confirm the role of sea ice anomalies on the atmospheric circulation.

4. Conclusions

In this study, we investigate the characteristics and potential large-scale causes of the devastating heatwave event in the western NA from late June to early July 2021. The analysis shows that the frequency of regional heatwaves and summer mean Tmax values are closely associated with the number of QBTR days over WNA in summer during 1980–2021. A direct cause of the 2021 record-breaking heatwave is an extended QBTR event over WNA lasting eight days.

Correlations of QBTRs with climate indices reveal a transition from AO modulation during 1980–2000 to a significant modulation by the sea ice concentrations in the Chukchi Sea during 2001–2021, reflecting the strengthened role of the Arctic sea ice variations. During the latter period (2001–2021), the negative sea ice anomalies in the Chukchi Sea, concurrent with stronger net surface shortwave radiation and increased near-surface air temperature, induce upward motion in the low- and mid-troposphere and a low-pressure center therein. The low-pressure center induces westerly anomalies on its southern flank, strengthening a stationary wave response, inducing more QBTRs over western NA. The more stationary QBTR events can cause an extended period of high temperatures over large regions of western NA compared to a more transient and smaller temperature increase caused by the QBCR events. Therefore, heatwaves over western NA are more likely to occur with increased barotropic and long-lived ridge events. The observations in the past two decades suggest that negative Arctic sea ice anomalies triggers more QBTR events. Since the Arctic sea ice is projected to continue to decline under global warming (Stroeve *et al* 2012, Overland and Wang 2013, Notz and Community 2020), as a result, the frequency of heatwaves in summertime over western NA is likely to increase, potentially leading to more wildfires in the region.

Data availability statement

All data used in this study is publicly available, including ERA5 data on single levels (https://cds.climate.copernicus.eu/cdsapp#!/dataset/reanalysis-era5-single-levels-preliminary-back-extension?tab=overview) and pressure levels (https://cds.climate.copernicus.eu/cdsapp#!/dataset/reanalysis-era5-pressure-levels?tab=overview), sea ice concentration at Met Office Hadley Centre (www.metoffice.gov.uk/hadobs/hadisst/data/download.html), and monthly AO index from Climate Prediction Center (www.cpc.ncep.noaa.gov/products/precip/CWlink/daily_ao_index/ao.shtml).

All data that support the findings of this study are included within the article (and any supplementary files).

Acknowledgments

This research was supported by the National Key R&D Program of China (2022YFE0106400) and Fundamental Research Funds for the Central Universities (202072001). Y W was supported by the National Science Foundation Atmospheric Chemistry Program.

Conflict of interest

The authors declare that they have no conflict of interest.

References

Barriopedro D, Fischer E M, Luterbacher J, Trigo R M and García-Herrera R 2011 The hot summer of 2010: redrawing the temperature record map of Europe *Science* **332** 220–4

Bondur V G 2011 Satellite monitoring of wildfires during the anomalous heat wave of 2010 in Russia *Izv. Atmos. Ocean. Phys.* **47** 1039–48

Budikova D, Ford T W and Ballinger T J 2019 United States heat wave frequency and Arctic Ocean marginal sea ice variability *J. Geophys. Res.* **124** 6247–64

Cavalieri D J and Parkinson C L 2012 Arctic sea ice variability and trends, 1979–2010 *Cryosphere* **6** 881–9

Chang E K M 2009 Diabatic and orographic forcing of Northern winter stationary waves and storm tracks *J. Clim.* **22** 670–88

Coumou D, Di Capua G, Vavrus S, Wang L and Wang S 2018 The influence of Arctic amplification on mid-latitude summer circulation *Nat. Commun.* **9** 2959

Coumou D, Lehmann J and Beckmann J 2015 The weakening summer circulation in the Northern Hemisphere mid-latitudes *Science* **348** 324–7

Cvijanovic I, Santer B D, Bonfils C, Lucas D D, Chiang J C H and Zimmerman S 2017 Future loss of Arctic sea-ice cover could drive a substantial decrease in California's rainfall *Nat. Commun.* **8** 1947

Du Y, Zhang J, Zhao S and Chen Z 2022 A mechanism of spring Barents Sea ice effect on the extreme summer droughts in northeastern China *Clim. Dyn.* **58** 1033–48

Fischer E M, Seneviratne S I, Vidale P L, Lüthii D and Schär C 2007 Soil moisture–atmosphere interactions during the 2003 European summer heat wave *J. Clim.* **20** 5081–99

Francis J A and Vavrus S J 2012 Evidence linking Arctic amplification to extreme weather in mid-latitudes *Geophys. Res. Lett.* **39** L06801

Gao Y, Fu J S, Drake J B, Liu Y and Lamarque J F 2012 Projected changes of extreme weather events in the eastern United States based on a high resolution climate modeling system *Environ. Res. Lett.* **7** 044025

Gao Y, Leung L R, Lu J and Masato G 2015 Persistent cold air outbreaks over North America in a warming climate *Environ. Res. Lett.* **10** 044001

Habeeb D, Vargo J and Stone B 2015 Rising heat wave trends in large US cities *Nat. Hazards* **76** 1651–65

Hartmann D L 2015 *Global Physical Climatology* (Waltham, MA: Elsevier Science) p 182

He S, Gao Y, Furevik T, Wang H and Li F 2018 Teleconnection between sea ice in the Barents Sea in June and the silk road, Pacific–Japan and East Asian rainfall patterns in August *Adv. Atmos. Sci.* **35** 52–64

Hersbach H *et al* 2020 The ERA5 global reanalysis *Q. J. R. Meteorol. Soc.* **146** 1999–2049

Holton J R 2004 *An Introduction to Dynamic Meteorology* (Burlington, MA: Elsevier Academic Press) pp 60

Inoue J, Hori M E and Takaya K 2012 The role of Barents Sea ice in the wintertime cyclone track and emergence of a warm-Arctic cold-Siberian anomaly *J. Clim.* **25** 2561–8

Kim H, Yeh S-W, An S-I, Park J-H, Kim B-M and Baek E-H 2020 Arctic Sea ice loss as a potential trigger for central Pacific El Niño events *Geophys. Res. Lett.* **47** e2020GL087028

Knowlton K, Rotkin-Ellman M, King G, Margolis H G, Smith D, Solomon G, Trent R and English P 2009 The 2006 California heat wave: impacts on hospitalizations and emergency department visits *Environ. Health Perspect.* **117** 61–67

Kwok R and Rothrock D A 2009 Decline in Arctic sea ice thickness from submarine and ICESat records: 1958–2008 *Geophys. Res. Lett.* **36** L15501

Lackmann G 2011 *Midlatitude Synoptic Meteorology: Dynamics, Analysis, and Forecasting* (Boston, MA: American Meteorological Society) p 3

Li J, Ding T, Jia X and Zhao X 2015 Analysis on the extreme heat wave over China around Yangtze River region in the summer of 2013 and its main contributing factors *Adv. Meteorol.* **2015** 706713

Li M, Yao Y, Simmonds I, Luo D, Zhong L and Chen X 2020 Collaborative impact of the NAO and atmospheric blocking on European heatwaves, with a focus on the hot summer of 2018 *Environ. Res. Lett.* **15** 114003

Li Q, Huang Y, Fan Y, Tang S and Hu Y 2018 Automatic analysis of trough lines based on curvature tracing *Atmosphere* **9** 88

Nitta T 1987 Convective activities in the tropical Western Pacific and their impact on the Northern Hemisphere summer circulation *J. Meteorol. Soc. Japan* II **65** 373–90

Notz D and Community S 2020 Arctic Sea Ice in CMIP6 *Geophys. Res. Lett.* **47** e2019GL086749

Overland J E, Dethloff K, Francis J A, Hall R J, Hanna E, Kim S-J, Screen J A, Shepherd T G and Vihma T 2016 Nonlinear response of mid-latitude weather to the changing Arctic *Nat. Clim. Change* **6** 992–9

Overland J E and Wang M 2013 When will the summer Arctic be nearly sea ice free? *Geophys. Res. Lett.* **40** 2097–101

Pearce A F and Feng M 2013 The rise and fall of the 'marine heat wave' off Western Australia during the summer of 2010/2011 *J. Mar. Syst.* **111–112** 139–56

Pelly J L and Hoskins B J 2003 A new perspective on blocking *J. Atmos. Sci.* **60** 743–55

Sánchez-Benítez A, García-Herrera R, Barriopedro D, Sousa P M and Trigo R M 2018 June 2017: the earliest European summer mega-heatwave of reanalysis period *Geophys. Res. Lett.* **45** 1955–62

Schaller N, Sillmann J, Anstey J, Fischer E M, Grams C M and Russo S 2018 Influence of blocking on Northern European and Western Russian heatwaves in large climate model ensembles *Environ. Res. Lett.* **13** 054015

Schiermeier Q 2021 Climate change made North America's deadly heatwave 150 times more likely *Nature* (https://doi.org/10.1038/d41586-021-01869-0)

Screen J A and Simmonds I 2010 The central role of diminishing sea ice in recent Arctic temperature amplification *Nature* **464** 1334–7

Screen J A, Simmonds I, Deser C and Tomas R 2013 The atmospheric response to three decades of observed Arctic Sea Ice loss *J. Clim.* **26** 1230–48

Slingo A and Slingo J M 1988 The response of a general circulation model to cloud longwave radiative forcing. I: introduction and initial experiments *Q. J. R. Meteorol. Soc.* **114** 1027–62

Small D, Atallah E and Gyakum J R 2014 An objectively determined blocking index and its Northern Hemisphere *Climatol. J. Clim.* **27** 2948–70

Smoyer-Tomic K E, Kuhn R and Hudson A 2003 Heat wave hazards: an overview of heat wave impacts in Canada *Nat. Hazards* **28** 465–86

Stefanon M, D'Andrea F and Drobinski P 2012 Heatwave classification over Europe and the mediterranean region *Environ. Res. Lett.* **7** 014023

Strey S T, Chapman W L and Walsh J E 2010 The 2007 sea ice minimum: impacts on the Northern Hemisphere atmosphere in late autumn and early winter *J. Geophys. Res.* **115** D23103

Stroeve J C, Kattsov V, Barrett A, Serreze M, Pavlova T, Holland M and Meier W N 2012 Trends in Arctic sea ice extent from CMIP5, CMIP3 and observations *Geophys. Res. Lett.* **39** L16502

Teng H, Branstator G, Wang H, Meehl G A and Washington W M 2013 Probability of US heat waves affected by a subseasonal planetary wave pattern *Nat. Geosci.* **6** 1056–61

Thompson D W J and Wallace J M 2000 Annular modes in the extratropical circulation. Part I: month-to-month variability *J. Clim.* **13** 1000–16

Vihma T 2014 Effects of Arctic Sea Ice decline on weather and climate: a review *Surv. Geophys.* **35** 1175–214

von Biela V R, Arimitsu M L, Piatt J F, Heflin B, Schoen S K, Trowbridge J and Clawson C 2019 Extreme reduction in nutritional value of a key forage fish during the Pacific marine heatwave of 2014–2016 *Mar. Ecol. Prog. Ser.* **613** 171–82

Wallace J M and Hobbs P V 2006 *Atmospheric Science: An Introductory Survey* (Amsterdam: Elsevier) pp 88–93

Wang H and He S 2015 The North China/Northeastern Asia severe summer drought in 2014 *J. Clim.* **28** 6667–81

Yao Y, Luo D, Dai A and Simmonds I 2017 Increased quasi stationarity and persistence of winter ural blocking and Eurasian extreme cold events in response to Arctic warming. Part I: insights from observational analyses *J. Clim.* **30** 3549–68

Yeo S-R, Kim K-Y, Yeh S-W, Kim B-M, Shim T and Jhun J-G 2014 Recent climate variation in the bering and Chukchi Seas and its linkages to large-scale circulation in the Pacific *Clim. Dyn.* **42** 2423–37

Yin Z, Wang H, Li Y, Ma X and Zhang X 2019b Links of climate variability in Arctic sea ice, Eurasian teleconnection pattern and summer surface ozone pollution in North China *Atmos. Chem. Phys.* **19** 3857–71

Yin Z, Wang H and Ma X 2019a Possible relationship between the Chukchi Sea Ice in the early winter and the February haze pollution in the North China plain *J. Clim.* **32** 5179–90

Yin Z, Yuan D, Zhang X, Yang Q and Xia S 2020 Different contributions of Arctic sea ice anomalies from different regions to North China summer ozone pollution *Int. J. Climatol.* **40** 559–71

Zhang J, Gao Y, Luo K, Leung L R, Zhang Y, Wang K and Fan J 2018 Impacts of compound extreme weather events on ozone in the present and future *Atmos. Chem. Phys.* **18** 9861–77

Zou Y, Rasch P J, Wang H, Xie Z and Zhang R 2021 Increasing large wildfires over the western United States linked to diminishing sea ice in the Arctic *Nat. Commun.* **12** 6048

Zou Y, Wang Y, Xie Z, Wang H and Rasch P J 2020 Atmospheric teleconnection processes linking winter air stagnation and haze extremes in China with regional Arctic sea ice decline *Atmos. Chem. Phys.* **20** 4999–5017